Transition-metal doping of semiconducting chalcopyrites: half-metallicity and magnetism

2007 J. Phys.: Condens. Matter 19 016210

(http://iopscience.iop.org/0953-8984/19/1/016210)

INSTITUTE OF PHYSICS PUBLISHING JOURNAL OF PHYSICS: CONDENSED MATTER

J. Phys.: Condens. Matter **19** (2007) 016210 (13pp) doi:10.1088/0953-8984/19/1/016210

Transition-metal doping of semiconducting chalcopyrites: half-metallicity and magnetism

Sergey Y Sarkisov[1] **and Silvia Picozzi**[2]

[1] Russian Academy of Science, Siberian Branch, Inst. Monitoring Climat. and Ecol. Syst., 634055 Tomsk, Russia
[2] CNR-INFM, CASTI Regional Laboratory, 67010 Coppito (L'Aquila), Italy

E-mail: silvia.picozzi@aquila.infn.it

Received 25 October 2006, in final form 14 November 2006
Published 7 December 2006
Online at stacks.iop.org/JPhysCM/19/016210

Abstract

An extensive *ab initio* investigation of the electronic and magnetic structure of transition-metal-doped chalcopyrites is reported, focusing on Cr, Mn and Fe in $CuAlS_2$, $AgGaS_2$, $ZnGeP_2$ and $CdGeAs_2$. Our results show that the electronic properties, in terms of defect-induced density of states, largely depend on the specific combination of host, transition-metal dopant and substituted cation. In particular, for $AgGaS_2$ doped with Cr, Mn and Fe in both cationic sites, we show that the transition metal substituting silver gives rise to strongly localized orbitals in proximity to the Fermi level, whereas generally a much higher hybridization occurs when the transition metal substitutes for Ga. On the other hand, if we fix the dopant, namely Cr, and introduce it into different hosts, Cr-doped $CuAlS_2$ and $AgGaS_2$ show more localized defect-induced states, whereas in more covalently bonded hosts, such as $ZnGeP_2$ and $CdGeAs_2$, a stronger hybridization between Cr d states and the host valence band occurs. Our findings have important consequences on the exchange interaction range, that, along with the exchange interaction strength, must be taken into account in a careful materials design aiming at optimizing the ferromagnetic properties. Finally, exploiting a simple model to predict magnetic moments in diluted magnetic semiconductors, we achieve half-metallic antiferromagnetism in chalcopyrites by co-doping $CuAlS_2$ with Mn and V; indeed, we obtain a 100% spin-polarized density of states, with a mixed impurity band due to both Mn and V d states, ferrimagnetically coupled in the ground state.

(Some figures in this article are in colour only in the electronic version)

1. Introduction

Ever since the discovery of ferromagnetism persisting up to relatively high temperatures (<170 K) in the diluted magnetic semiconductor (DMS) prototype, i.e. Mn-doped GaAs,

transition-metal (TM) doping of semiconductors (SCs) has attracted increasing interests [1, 2]. In particular, substantial attention has been devoted to ternary semiconductors with chalcopyrite (CH) structure (i.e. ternary analogues of zinc blende binary compounds) alloyed with magnetic impurities, due to their presumed ferromagnetism persisting up to room temperature [4]. Taking into account the appealing nonlinear optical properties of pure chalcopyrites and their characteristics promising for photovoltaic devices [3], new applications in opto-electronics or magneto-optics, based on the manipulation of the magnetic state by light can be envisaged, which contribute to making this class of compound particularly promising.

In addition to the potentially relevant technological applications and to the interesting experimental results [5], it is interesting from the fundamental point of view to focus on the electronic properties of diluted magnetic chalcopyrites (DMCHs), i.e. different chalcopyrites doped with several transition metals. As is well known, there are two kinds of chalcopyrite: II–IV–V_2 [6] and I–III–VI_2. The first class represents the ternary analogue of a III–V SC, where the element of the third column is substituted by an element of the second and fourth column, alternately. Similarly, the second class of chalcopyrite is the ternary counterpart of the II–VI SC, where the cation is substituted by an element of the first and of the third column, alternately. Therefore, ternaries offer a vast playground for achieving different electronic and magnetic properties, due to the wide variety of sites where the TM can be doped: in fact, a TM can substitute for II and IV sites in the first class of CH and for the I and III sites in the second class of CH. In this respect, different TMs, with their correspondingly different number of d electrons, can have different valence states when substituted in the same CH site. In parallel, the different sites allowed by the two classes of CH, each having two possible cationic sites with their corresponding oxidation states, can impart different electronic properties to the same TM impurity.

The intrinsic CH variety suggests using them as SC host for achieving 'half-metallic (HM) antiferromagnetism', a special case of ferrimagnetism (FiM) with compensated magnetic moment and 100% spin-polarization at the Fermi level. This concept was originally proposed in [17] and applied by means of *ab initio* simulations to double-perovskites [19], Heusler alloys [20] and very recently applied in the DMS framework [18]: it is based on the particular case of a ferrimagnetic coupling between two different TMs, that give rise to an overall zero magnetization. Half-metallic ferrimagnets might be important from the technological point of view: since they do not have stray fields and are only slightly influenced by external magnetic fields, they could be used as sensors in measuring the spin-polarization via spin-resolved scanning tunnelling microscopy, taking advantage of the fact that they do not alter the magnetic domains. However, the experimental proof that HM-FiM exists in nature is still lacking, possibly due to atomic disorder in real samples that induces changes with respect to first-principles electronic structure predictions.

Within the wide variety of DMCHs, several different theoretical works have been carried out, both in II–IV–V_2 [9, 11–13] and I–III–VI_2 classes [7, 8, 10]. In particular, of main interest for the present investigation are the following first-principles findings. (i) It was shown for I–III–VI_2 [7], that Mn doping at the III site stabilizes a ferromagnetic (FM) ground state, providing holes and in agreement with either double-exchange for more 'ionic' compounds or the generally accepted hole-mediated ferromagnetic exchange interaction proposed by Dietl and co-workers [1] for more 'covalent' hosts. On the other hand, Mn doping at the I site provides electrons, but still gives rise to a predominantly FM interaction. From the energetics point of view, the Mn favoured site—as well as the host stability itself—strongly depends on the Cu and Mn chemical potentials. (ii) Cr (Mn and Fe) substituting the first cation in II–IV–V_2 were found to give rise to FM (AFM) coupling, whereas Cr and Mn (Fe) substituting the first cation in I–III–VI_2 were found to stabilize an FM (AFM) ground state [8]. In addition,

Table 1. Relevant experimental structural parameters for the host chalcopyrites: in-plane lattice constant (a, in au), out-of-plane lattice constant (c, in au), c/a ratio, and internal structural parameter (u).

	a	c	c/a	u
$CuAlS_2$ [a]	10.06	19.73	1.96	0.27
$AgGaS_2$ [a]	10.88	19.43	1.79	0.29
$ZnGeP_2$ [b]	10.32	20.22	1.96	0.26
$CdGeAs_2$ [c]	11.23	21.21	1.89	0.28

[a] Reference [14]; [b] Reference [15]; [c] Reference [16].

Cr-doped $CuAlS_2$ and $AgGaS_2$ were predicted to have a remarkably high Curie temperature T_C (well above room temperature), although the estimate was based on a mean-field theory which is well known to overestimate T_C [8].

On the basis of these previous works, we carried out a systematic investigation of Cr, Mn and Fe in four different CHs, namely $CuAlS_2$, $AgGaS_2$, $ZnGeP_2$ and $CdGeAs_2$, representative of both I–III–VI_2 and II–IV–V_2 classes and for the majority of which a thorough discussion of the first-principles electronic structure is lacking. In particular, after reporting some technicalities in section 2, we recall in section 3 the commonly accepted model used to predict the magnetic moment in DMSs, applied to the CH framework; in section 4 we explicitly show the results of our simulations in terms of density of states for (i) $AgGaS_2$ doped with different TMs (section 4.1) and (ii) Cr doped in the different CHs (section 4.2). In the second part of the paper, we focus on the possibility to achieve half-metallicity in ferrimagnetically doped CHs, and in particular in $CuAlS_2$ co-doped with Mn and V (see section 5). In section 6 we summarize our main findings.

2. Technical details

Our simulations were performed within the density functional theory (DFT), using the generalized gradient approximation [22] to the exchange–correlation potential and the all-electron full-potential linearized augmented plane wave (FLAPW) method [23] in the FLEUR implementation [24]. Our simulations were carried out within the scalar relativistic approximation (i.e. spin–orbit coupling was neglected, since it is believed to be generally small and not to affect the main underlying physics) and in the collinear-spins framework. Muffin-tin radii have been chosen as 2.33 au (Cu), 2.05 au (S, Al), 2.28 au (Mn, Cr, Fe, Zn), 2.65 au (Ag), 2.09 au (Ga), 2.43 au (Cd), 2.14 au (Ge, P), and 2.03 au (As). The wavefunction in the interstitial region was expanded in plane waves using wavevectors up to 3.7 au^{-1}. The Brillouin zone sampling was performed using the $6 \times 6 \times 3$ Monkhorst–Pack shell [25].

As far as the structural parameters are concerned, we used a 16-atom unit cell, schematically shown in figure 1 in the case of Mn-doped $CuAlS_2$. The experimental lattice constants for the different CH hosts were used in the simulations (see table 1). We considered one TM (i.e. 25% dopant concentration) per unit cell, that substitutes both possible cationic sites: I and III in the I–III–VI_2 CH and II and IV in the II–IV–V_2 CH.[3] In each configuration, the TM is four-fold coordinated to four anions, forming a compressed tetrahedron along the c-axis. We checked that the electronic properties are only weakly perturbed by the atomic relaxations and so, in the following, we will focus on the unrelaxed structures. As far as

[3] The theoretical evaluation of defect formation energies of different TMs in different chalcopyrites and in different cationic sites goes beyond the scope of the present work. For Mn in several chalcopyrites, we refer to the work of Zunger and co-workers (see [9] and [7]).

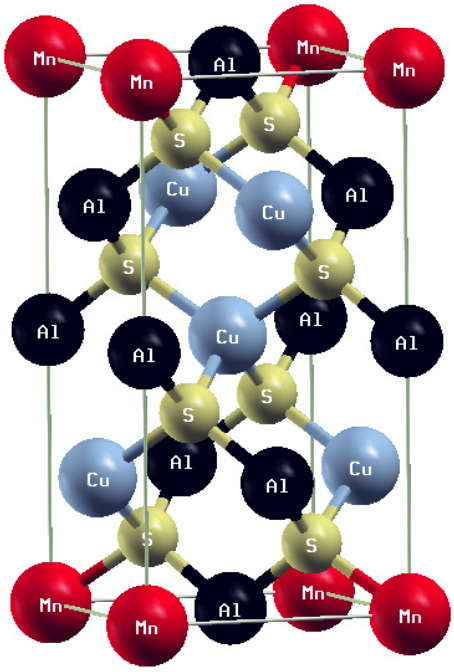

Figure 1. Schematic tetragonal unit cell for transition-metal-doped chalcopyrites (here, we show Mn-doped $CuAlS_2$ containing 16 atoms). Mn, Cu, Al and S atoms are shown by red, grey, black and yellow spheres in the electronic version.

the HM-AFM system is concerned, we considered a 32-atom $CuAlS_2$ unit cell with the two different TMs substituting the Cu site, one at the origin and the other in $(0, a, 0)$.

3. Magnetic moment prediction: a simple model

Let us briefly recall the mechanism that acts when doping a semiconductor with a TM impurity. In a perfect tetrahedral environment, the TM d states split by exchange in majority and minority states and by the crystal field in two-fold-degenerate e and three-fold-degenerate t_2 orbitals. However, in a chalcopyrite crystal, due to the c/a ratio and to the x parameter being different from ideal parameters of 2 and 1/4, respectively, the e states further split in d_{z^2} and $d_{x^2-y^2}$, whereas the d_{xz} and d_{yz} split from the d_{xy} orbitals. In any case, we will continue to use the e and t nomenclature, which is strictly not correct in the CH context, but it is commonly used in DMSs and will serve as comparison with corresponding well-studied TM-doped binary semiconductors. The t states very efficiently hybridize with host anion p states, giving rise to bonding and antibonding orbitals, whereas the e states show a non-bonding and well-localized character (except in some cases; see below). From the occupation point of view, the bonding majority t_+ and minority t_- states are always filled, whereas the antibonding minority states are always empty. On the other hand, the occupation of the other relevant orbitals close to the Fermi level can change depending on the TM and host. Of particular relevance are partially filled orbitals that give rise to holes (or electrons, in principle), since they are believed to be responsible for the celebrated carrier-mediated ferromagnetism in DMSs [1].

According to the previous model and taking into account the available electrons of the TM and from the host, we report in table 2 the predicted properties of different TMs in different

Table 2. TM (namely, Cr, Mn and Fe) nominal d electron configuration, relevant occupied states and resulting magnetic moment (in Bohr magnetons) for TMs substituting element I and III in I–III–VI_2 and element II and IV in II–IV–V_2 chalcopyrites. Bonding (anti-bonding) t states in the majority (minority) channel are always filled (empty) and are therefore not explicitly reported.

	d configuration				Occupied states				Magn. moment			
	I	II	III	IV	I	II	III	IV	I	II	III	IV
Cr	d^5	d^4	d^3	d^2	$e^2_+ t^3_+$	$e^2_+ t^2_+$	$e^2_+ t^1_+$	e^2_+	5	4	3	2
Mn	d^6	d^5	d^4	d^3	$e^2_+ t^3_+ e^1_-$	$e^2_+ t^3_+$	$e^2_+ t^2_+$	$e^2_+ t^1_+$	4	5	4	3
Fe	d^7	d^6	d^5	d^4	$e^2_+ t^3_+ e^2_-$	$e^2_+ t^3_+ e^1_-$	$e^2_+ t^3_+$	$e^2_+ t^2_+$	3	4	5	4

Table 3. Total (μ_{tot}) and TM (μ_{TM}) magnetic moment in different TM-doped CHs (16-atom unit cell). Values in Bohr magnetons.

	Cr_I		Cr_{II}		Cr_{III}		Cr_{IV}	
	$CuAlS_2$	$AgGaS_2$	$ZnGeP_2$	$CdGeAs_2$	$CuAlS_2$	$AgGaS_2$	$ZnGeP_2$	$CdGeAs_2$
μ_{tot}	5.00	5.00	4.00	3.97	3.00	3.01	2.00	2.00
μ_{TM}	3.72	3.71	2.98	3.36	2.57	2.60	2.03	2.21
	Mn_I		Mn_{II}		Mn_{III}		Mn_{IV}	
	$CuAlS_2$	$AgGaS_2$	$ZnGeP_2$	$CdGeAs_2$	$CuAlS_2$	$AgGaS_2$	$ZnGeP_2$	$CdGeAs_2$
μ_{tot}	4.00	4.22	4.99	5.00	4.00	4.00	3.00	3.00
μ_{TM}	3.38	3.73	3.69	4.00	3.42	3.49	2.91	3.08
	Fe_I		Fe_{II}		Fe_{III}		Fe_{IV}	
	$CuAlS_2$	$AgGaS_2$	$ZnGeP_2$	$CdGeAs_2$	$CuAlS_2$	$AgGaS_2$	$ZnGeP_2$	$CdGeAs_2$
μ_{tot}	3.00	3.07	3.91	4.00	4.92	4.98	2.78	3.26
μ_{TM}	2.51	2.75	2.93	3.15	3.26	3.39	2.46	3.50

sites, in terms of the nominal number of d electrons, occupied orbitals and resulting magnetic moment. The validity of the model is confirmed by many previous *ab initio* results [27], in terms of calculated magnetic moments and energy ordering of different orbitals. Our first-principles simulations, as well, are in agreement with the model predictions, as explicitly shown in table 3, the only notable exception being Fe in the IV position in II–IV–V_2 CH, where the moment ($\sim$2–3 μ_B) is lower than predicted (4 μ_B). Several reasons might be responsible for this unexpected trend, among which we mention (i) the exchange splitting, that in Fe could be not large enough to overcome the crystal-field splitting, so that Fe is found to be in a low-spin state, or (ii) some computational parameters, such as the relatively small unit cell considered, parameterization of the exchange–correlation potential, **k**-point sampling, atomic relaxations, etc that might affect this 'off-trend' value.

Despite the undiscussed validity and the general character of the model, first-principles calculations are needed in order to establish the position of the TM-induced states with respect to the band edges. In fact, this affects the nature of the exchange mechanism (i.e. Zener p–d exchange versus double-exchange) and, in turn, the long-range versus short-range character of the magnetic interaction. The results of our simulations will be therefore explicitly reported in the following section, focusing especially on the density of states. It is useful to analyse in

a careful way the symmetry breaking of the t_2 and e orbitals, due to the tetragonal distortion (especially in $AgGaS_2$ and $CdGeAs_2$) and their consequent hybridization which in turn affects the effective localization of the TM d orbitals. We would like to remark that, due to the sometimes inaccurate treatment of correlation effects within bare DFT, the position of the d states may not correspond to the one experimentally realized. Several artefacts may be used to correct this error, including the so-called LDA + U approach [26], where two parameters, the Hubbard U and Hund J, are introduced as external inputs to treat correlated d states in a Hubbard-like way. However, so far, there is no consensus on the values of U and J for TMs in DMSs. In addition, U and J might of course be different for different TMs or different hosts and should be chosen according to spectroscopic experiments, that are often lacking for DMCHs. In the present work, therefore, we will limit our discussion to the standard generalized gradient approximation GGA-DFT approach, so as to treat all the different hosts and dopant situations in a consistent way.

4. Single impurities in transition-metal-doped chalcopyrites: half-metallicity and defect-induced gap states

4.1. Different transition-metal impurities in the same host

Let us start the discussion of the electronic properties of three different TMs (namely, Cr, Mn and Fe) in $AgGaS_2$ by focusing on the total density of states (TDOS) of the doped CH and of the pristine host, as well as on the density of states projected (PDOS) on the TM, reported in figure 2. Although—as previously pointed out—we do not focus on the magnetic ground state, we expect double-exchange rather than Zener p–d exchange to be the dominant mechanism to lead to a ferromagnetic coupling, due to the wide-gap character of $AgGaS_2$ and the related presence of an 'impurity band'. In the following, therefore, our predictions concerning the magnetic stability will be mostly performed in terms of double-exchange.

We recall that, according to Zunger [21], the p–d hybridization produces bonding–antibonding states, often referred as (1) crystal-field resonance (CFR) showing a very strong d (and therefore essentially localized) character, and (2) dangling-bond hybrid (DBH), showing a 'vacancy–host' character (and therefore a more delocalized behaviour). What determines whether the CFR has a higher or lower energy than the DBH? Basically, it depends on the ionicity of the host with respect to the dopant, as well as from the site where the TM is located. In particular, as previously pointed out, the character of the partially filled antibonding hybrids largely determines the related magnetic coupling: in the case of a partially filled DBH, the carriers reside essentially in a delocalized state and the magnetic interaction between two TM impurities can be effective over large TM–TM distances. On the other hand, in the case where the carriers are located in a CFR orbital, the nearest-neighbour couplings are expected to be high, but the resulting magnetic interaction typically shows a short-range behaviour. Indeed, the different mechanisms can be found in figure 2, where TM-induced states are evidenced by means of the comparison with the host-like TDOS. As a general remark, we note that, focusing on the majority PDOS, when Cr substitutes the first cation, a strongly CFR-like orbital is closer to E_F, whereas when it substitutes for the second cation, there is a much more mixed situation and Cr shows a much broader PDOS which cannot be really ascribed more to TM d character rather than to SC anion p states. This is consistent with what is proposed in [7], where the authors observed a reversed ordering for Mn substituting Cu or Al in $CuAlS_2$ and attributed the different behaviour to the host dangling bonds produced by a Cu vacancy being deeper in energy (i.e. located below the SC valence band maximum, VBM) than those induced by an Al vacancy (i.e. located above the VBM). Furthermore, most of the features

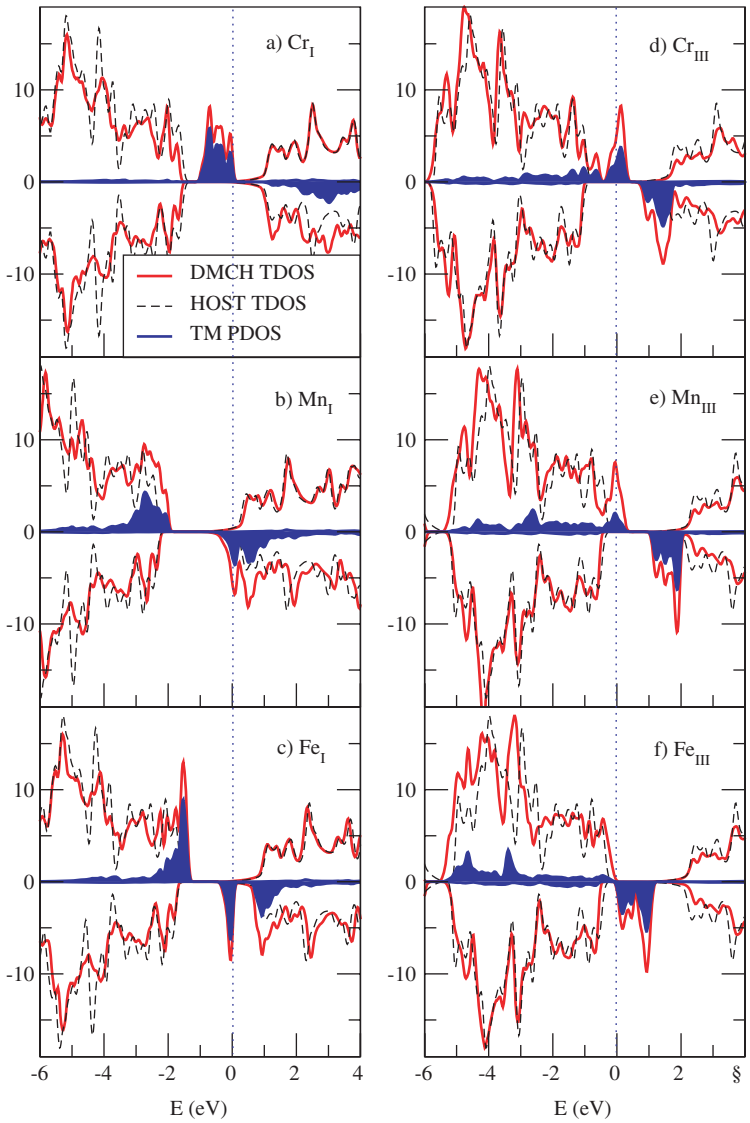

Figure 2. Density of states for TM-doped $AgGaS_2$: (a) $Cr_xAg_{1-x}GaS_2$, (b) $Mn_xAg_{1-x}GaS_2$, (c) $Fe_xAg_{1-x}GaS_2$, (d) $AgCr_xGa_{1-x}S_2$, (e) $AgMn_xGa_{1-x}S_2$ and (f) $AgFe_xGa_{1-x}S_2$. The solid bold (red), dashed and grey (blue) lines show the TDOS for the DMCH, the TDOS for the host and the PDOS for the TM dopant, respectively. The TDOS of the host was arbitrarily shifted in energy along the x-axis so as to make the relevant peaks coincide with the doped system. Majority and minority states are shown in the positive and negative y-axis, respectively. The Fermi level is set to zero in the energy scale.

present in the TM-doped CH TDOS are reminiscent of the host TDOS, with the exception of states that are present in the gap or in proximity to the Fermi level, E_F. This is particularly evident in the case of $Cr_xAg_{1-x}GaS_2$ (see figure 2(a)) and in $AgFe_xGa_{1-x}S_2$ (see figure 2(f)) in the majority and minority spin channels, respectively. Recall that these systems show a total magnetic moment of $\sim 5\ \mu_B$; the t_+^b and t_-^{ab} are either fully occupied or fully empty. In this case, the Fermi level does not lie within an impurity band, so the double-exchange

energy gain does not occur and ferromagnetism is not predicted. In the other cases, the TM-induced states are close to one of the band edges. For example, in the $AgCr_xGa_{1-x}S_2$ and $AgMn_xGa_{1-x}S_2$ (cf figures 2(e) and (f), respectively) the majority spin states cross E_F (and are therefore partially occupied), whereas the minority states are close to the conduction band maximum (CBM) (but they are completely unoccupied). In these two cases, our calculated total moment is 3 μ_B and 4 μ_B, respectively, and the expected coupling is FM, since this is expected to be stabilized by double-exchange. On the other hand, $Fe_xAg_{1-x}GaS_2$ (see figure 2(c)) shows TM-induced states close to the VBM in the majority spins, whereas a mid-gap state is present in the minority spins case. In this case, there are not partially occupied states (as shown in table 2 and confirmed by the DOS in figure 2(c)). In the latter case, we do not expect hole-induced FM, because no energy gain is expected via double-exchange. Finally, $Mn_xAg_{1-x}GaS_2$ (cf figure 2(b)) shows dopant-induced states close to both the VBM and the CBM edges, in the up and down spin channels, respectively. Although, for this latter system, exchange coupling constants have not been calculated, in similar situations where the occupancy is e^1_- (such as I–Co_xIII_{1-x}–VI_2 or Fe_xII_{1-x}–IV–V_2, where explicit DFT calculations were carried out [8]), the spin-glass state was realized. The reason is that, although E_F lies in an impurity band, this is an e-like orbital and, as such, rather localized, so the efficiency with which double-exchange occurs is low and the spin-glass state is found to be the ground state. A similar situation might occur here for $Mn_xAg_{1-x}GaS_2$.

Finally, we briefly comment on the half-metallicity, since this is important from the technological point of view in the context of spin injection. As a result of the different energy positions of the gap-induced states, the TM doping often gives rise to half-metallicity. In particular, $AgCr_xGa_{1-x}S_2$ and $AgMn_xGa_{1-x}S_2$ are half-metallic (with the majority bands metallic) and $Mn_xAg_{1-x}GaS_2$ shows half-metallicity (with the minority bands metallic). On the other hand, $Cr_xAg_{1-x}GaS_2$, $Fe_xAg_{1-x}GaS_2$ and $AgFe_xGa_{1-x}S_2$ show a semiconducting behaviour for both spin channels.

4.2. Same transition-metal impurities in different hosts

In the previous section, we focused on $AgGaS_2$ doped with several transition metals, where we expect double-exchange to be the dominating mechanism, due to the large gap and the consequent high probability that an impurity band forms in it. On the other hand, we here focus on changing the host at fixed TM (namely Cr), moving progressively from a highly ionic host (such as $CuAlS_2$) to a more covalent compound (such as $CdGeAs_2$). In this case, we expect a transition from a double-exchange to a Zener p–d regime, all leading to FM but with different interaction ranges.

In figure 3 we report the orbital-resolved density of states for Cr in all the considered CHs and in both cationic sites, in order to compare the different mechanism of hybridization of Cr d states when doping different hosts and with distinct nominal valencies. As a general remark and as previously pointed out, we note that the reduced symmetry in the CH markedly splits the three-fold t and two-fold e states of a perfect tetrahedral environment. In many cases, we also note an e–t hybridization (as evident from the coincident energy positions for e and t orbitals in figure 3), which is symmetry allowed in CH, at variance with the case of a perfect zinc blende crystal at the Brillouin zone centre.

Let us now consider the different features when Cr is introduced in the various hosts (at fixed dopant concentration) and first discuss Cr in the first cationic positions, moving from Cr substituting the I-, II-, III- and IV-column element. In the majority spins for $Cr_xAg_{1-x}GaS_2$ and $Cr_xCu_{1-x}AlS_2$ the t_+ peak close to E_F shows a very strong d character and is therefore a CFR state (fully occupied; see figures 3(a) and (c)). On the other hand, $Cr_xZn_{1-x}GeP_2$ and

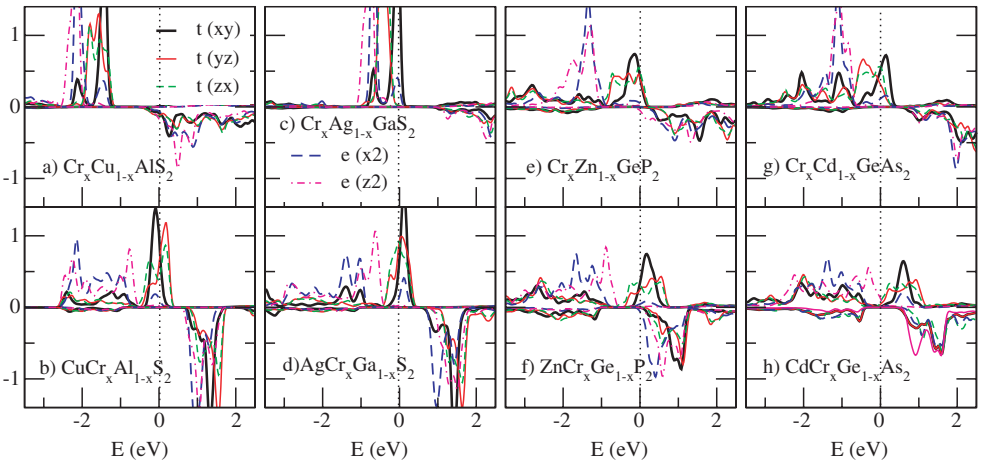

Figure 3. Orbital-resolved DOS for Cr in (a) I site in $CuAlS_2$, (b) III site in $CuAlS_2$, (c) I site in $AgGaS_2$, (d) III-site in $AgGaS_2$, (e) II site in $ZnGeP_2$, (f) IV site in $ZnGeP_2$, (g) II-site in $CdGeAs_2$ and (h) IV site in $CdGeAs_2$. The bold solid black, thin solid red, thin dashed green, bold dashed blue and dot–dashed pink line show the t_{xy}, t_{yz}, t_{zx}, $e_{x^2-y^2}$ and e_{z^2} orbitals, respectively. Majority and minority states are shown in the positive and negative y-axis, respectively.

$Cr_xCd_{1-x}GeAs_2$ (cf figures 3(e) and (g)) show a much higher hybridization and the peak close to E_F still shows a CFR character, but more delocalized than in the I–III–VI_2 CH. The e states always show a rather peaked feature, the fingerprint of an essentially non-bonding character. In the minority spin bands, the occupied states have a negligible contribution from the TM and are therefore DBH states, whereas the unoccupied states generally show a rather broad feature, with e and t states overlapped in energy. If we now move to the second cationic position, the e states appear much more strongly hybridized with t states. However, similar to Cr doped in the first cationic positions, $CuCr_xAl_{1-x}S_2$ and $AgCr_xGa_{1-x}S_2$ show a t_+ peak close to E_F with a CFR character, whereas it is more hybridized in both II–IV–V_2 CH hosts. In the down-spin channel both the e and t states are more peaked than for Cr in the first cationic position, still being the t_+ states occupied and with a marked DBH behaviour. Summarizing, among the configurations where FM is predicted (i.e. Cr in II–IV–V_2 substituting for the II-site and in I–III–VI_2 substituting for the III-site), the holes reside in a much more hybridized state in II–IV–V_2 CH. As a result, a longer-range FM interaction is expected in II–IV–V_2, compared to the more ionic I–III–VI_2 CH. On the other hand, the first-nearest-neighbour coupling in I–III–VI_2 is expected to be much stronger than in II–IV–V_2, as confirmed in similar situations for the III–Vs [28]. In addition, in moving from $ZnGeP_2$ to $CdGeAs_2$, there is an increased hybridization with the top of the valence band. Therefore, we cannot any longer speak of an 'impurity band', but rather it is more appropriate to describe TM-induced states as strongly hybridized with host-like valence bands. Finally, we point out that a tetragonal distortion of the host crystal (i.e. fixing the structural degrees of freedom) is not a sufficient factor to fully characterize a lower or higher e–t_2 hybridization or e splitting in x^2–y^2 or z^2 orbitals: for example, in Cr-doped $AgGaS_2$ there is a significative (negligible) symmetry breaking in $AgCr_xGa_{1-x}S_2$ ($Cr_xAg_{1-x}GaS_2$), depending on whether Cr substitutes for Ga or Ag. This confirms the importance of chemical and valency factors in predicting the final rearrangement of the electronic charge and, implicitly, outlines the relevance of first-principles calculations as a tool to predict the delicate interplay between chemical, electronic and structural degrees of freedom.

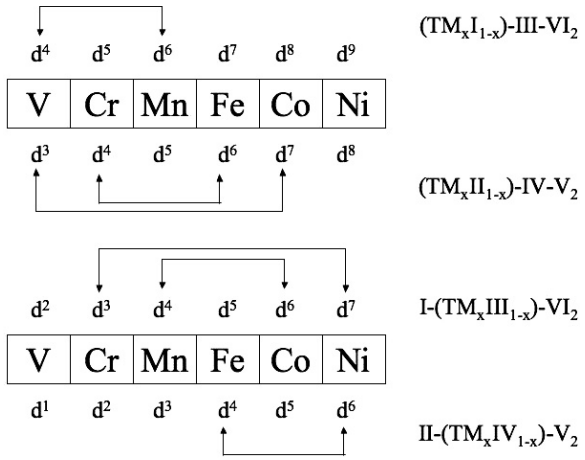

Figure 4. Schematics on co-doping in CHs: the different TMs (each with a different nominal d configuration) coupled by arrows are predicted to give rise to half-metallicity when antiferromagnetically aligned.

5. Transition-metal co-doping in chalcopyrites: half-metallic ferrimagnetism

According to the model proposed in section 3 and the different possibilities that can be realized in CHs, we expect that, by doping a CH with two specific different TMs, we might obtain a peculiar situation with a compensated magnetic moment. In particular, it was proposed in [18] that (i) one of the TMs should have more than half-filled d shell, whereas the other TM should have a less than half-filled d shell; (ii) the ferrimagnetic coupling should be stabilized via double-exchange, since a common band, originating from the two different TMs in proximity to E_F, should lead to a larger energy gain than the parallel spin-coupling, and (iii) the sum of the valence d electrons for the two TMs should be equal to 10. Therefore, in figure 4 we schematically show the most common magnetic TMs, along with their nominal d electron configuration in each of the considered CHs and in different cationic sites, and we show the different combinations that might give rise to HM-AFM.

Indeed, we choose one system, i.e. $CuAlS_2$, co-doped with Mn and V ferrimagnetically coupled, and verify from first principles that the predicted half-metallic ferrimagnetism is realized. In figure 5 we show the DOS for $Mn_xV_xCu_{1-2x}AlS_2$, in terms of the spin-resolved TDOS (panel (a)) and atom-resolved DOS on the V and Mn muffin tins (panels (c) and (d), respectively). As expected, full half-metallicity is present, with a metallic (semiconducting) character in the majority (minority) spin channels. In particular, the Mn and V PDOSs show that the impurity bands which give rise to half-metallicity are due to mixed Mn and V d states antiferromagnetically coupled.

Moreover, in figure 5(b) we show the integrated DOS, defined, for the majority spin channel, as $\mathrm{IDOS}^{\mathrm{up}}(E) = \int^E \mathrm{TDOS}^{\mathrm{up}}(E')\,\mathrm{d}E'$, corresponding to the number of electrons in the up spins (and, equivalently, for the down spins, integrating the minority spin TDOS). We also show $\mathrm{IDOS}^{\mathrm{tot}}$, i.e. the difference between the IDOS for the up and for the down spins, which of course leads to the total magnetic moment at $E = E_F$. It is interesting to note that the two contributions start differing at ~ -3.3 eV, where the strongly exchange-split Mn d states contribute to the minority TDOS. However, at ~ -1.4 eV the PDOS due to the Mn down spins becomes negligible and there is a plateau in the IDOS of about 1 eV. Approaching E_F and at ~ -1 eV, majority V d states start contributing, soon joined by Mn d up-spin states, and this

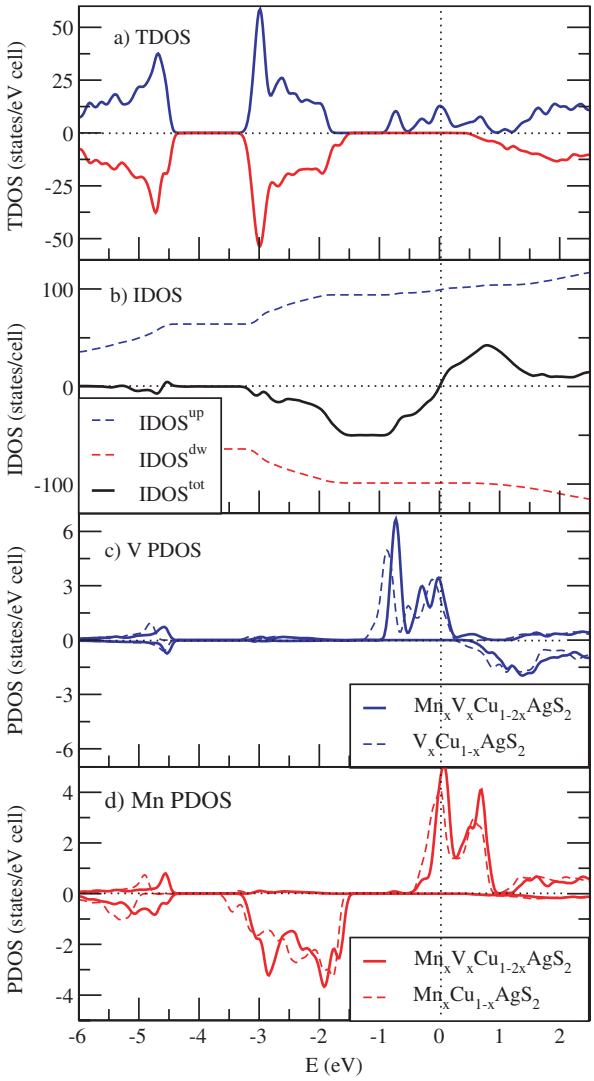

Figure 5. DOS for $Mn_xV_xCu_{1-2x}AlS_2$: (a) TDOS (the dark (blue) and light (red) lines show the majority and minority contributions, respectively); (b) IDOS (the dark (blue) and light (red) dashed lines show the majority and minority contributions, respectively) and the difference between the positive and negative contributions (black bold line); (c) and (d) show the V and Mn PDOSs, largely due to d states: solid (dashed) lines show the contributions in $Mn_xV_xCu_{1-2x}AlS_2$ ($V_xCu_{1-x}AlS_2$ (blue) and $Mn_xCu_{1-x}AlS_2$ (red), respectively). Majority and minority states are shown in the positive and negative y-axis, respectively, and the zero of the energy scale is set to E_F. To better compare with the HM-AFM system, the up and down spins for the Mn PDOS in $Mn_xCu_{1-x}AlS_2$ (cf panel (d)) have been reported in the negative and positive axis, respectively.

positive contribution brings the moment to exactly zero at E_F (i.e. the expected compensated magnetic moment). Above the Fermi level, Mn d states in the majority spin channel continue to strongly contribute and the IDOS becomes positive with a peak at around 1 eV. It is interesting to compare how the two separate constituents, namely $Mn_xCu_{1-x}AlS_2$ and $V_xCu_{1-x}AlS_2$, modify their electronic structure when Mn and V are co-doped in $CuAlS_2$. To this end, we

Table 4. Magnetic moments in the $Mn_xV_xCu_{1-2x}AlS_2$ system (32-atom cell, with Mn and V ferrimagnetically coupled), as compared with the corresponding constituents $V_xCu_{1-x}AlS_2$ and $Mn_xCu_{1-x}AlS_2$ (16-atom cell). Values in Bohr magnetons.

	M_{tot}	M_{Mn}	M_V	$M_{S(Mn)}$	$M_{S(V)}$
$Mn_xV_xCu_{1-2x}AlS_2$	0.00	−3.68	2.69	−0.012	0.006
$V_xCu_{1-x}AlS_2$	4.00	—	2.61	—	0.01
$Mn_xCu_{1-x}AlS_2$	4.00	3.53	—	0.018	—

show in figures 5(c) and (d) the comparison between the TM PDOSs in the singly doped host, i.e. $Mn_xCu_{1-x}AlS_2$ and $V_xCu_{1-x}AlS_2$, and the co-doped $Mn_xV_xCu_{1-2x}AlS_2$ system. Moreover, in table 4 we report the magnetic moments per unit cell and projected in the muffin tins on the two TMs and on their nearest-neighbour S atoms. It is evident that there is a slight rearrangement of both the charge and spin distribution in the co-doped system, as shown by the different PDOS and magnetic moment. In both the singly doped and co-doped chalcopyrite, the S atoms have a moment parallel to the TM moment, at variance with what is generally obtained in other III–V DMSs (including the GaMnAs prototype), where the negative moment of the anion (antiparallel to the TM moment) is believed to be a signature of the carrier-mediated Zener p–d interaction.

Finally, in order to countercheck the efficiency of an AFM-exchange mechanism, we verified that the ferrimagnetic alignment is the ground state and quantitatively estimated its stability: according to our results, the HM-AFM system (i.e. 32 atoms per cell, with one Mn and one V atom) is of the order of 100 meV lower in energy than the same system with Mn and V ferromagnetically coupled. Confirming what is proposed in [18], we can give a rationale of this result in terms of the different exchange mechanisms involved: in DMSs (and in the present case, as well), there is general competition between super-exchange and double-exchange. Here, however, double-exchange leads to ferrimagnetic coupling, whereas super-exchange leads to FM coupling (at variance with most of the cases, where it produces AFM coupling). As far as the energy gain is concerned, we observe that, due to the common Mn and V d impurity band (see figure 5(a)), double-exchange produces hybridization between two nearly degenerate states, whereas super-exchange leads to a mixing between energetically separated states. As a result, the gain in band energy due to double-exchange is much larger than that due to super-exchange and the half-metallic configuration is therefore stabilized.

6. Conclusions

A systematic study of the electronic and magnetic structure of transition-metal impurities in different kinds of chalcopyrite has been carried out by means of density-functional-based methods: Cr, Mn and Fe have been considered as magnetic dopants for $CuAlS_2$, $ZnGeP_2$, $AgGaS_2$ and $CdGeAs_2$. Our results show that most of the magnetically doped chalcopyrites considered show half-metallicity. The magnetic moments can be predicted on the basis of a simple model; however, the position of the impurity-induced states with respect to the semiconducting band edges depends on the delicate interplay between structural, chemical, electronic and valency degrees of freedom of both host and dopant. For example, fixing $AgGaS_2$ as a host and changing the magnetic impurity, we find that the transition metal substituting for silver (gallium) generally gives rise to localized (hybridized) states in proximity to the Fermi level, with important consequences on the range of interaction for the magnetic exchange. Similarly, fixing Cr as a magnetic dopant, Cr d states hybridize strongly and weakly with the band edges of II–IV–V_2 and I–III–VI_2 chalcopyrites, respectively. Finally, we suggest

the possibility of achieving half-metallicity in chalcopyrites by transition-metal co-doping: by introducing Mn and V in $CuAlS_2$, the ferrimagnetic state is obtained as the ground state, showing a 100% spin-polarization at the Fermi level.

Acknowledgments

Support by INTAS Young Scientist Fellowship Ref. No. 05-109-4603 awarded to SYS is gratefully acknowledged. SYS acknowledges kind hospitality from CASTI CNR-INFM Regional Laboratory, where part of the present work was performed.

References

[1] Dietl T, Ohno H, Matsukura F, Cibert J and Ferrand D 2000 *Science* **287** 1019
Dietl T, Ohno H and Matsukura F 2001 *Phys. Rev.* B **63** 195205
[2] Mac Donald A H, Schiffer P and Samarth N 2005 *Nat. Mater.* **4** 195 and references therein
[3] See for examples Kurohawa (ed) 2003 *Proc. 3rd Conf. on Photovoltaic Energy Conversion, 2003 (Osaka, Japan)* (Piscataway, NJ: IEEE Press)
Negami T, Nishitani M, Kohara N, Yashimoto K and Wada T 1996 *Mater. Res. Soc. Symp. Proc.* **426** 278
[4] Medvedkin G A, Ishibashi T, Nishi T, Hayata K, Hasegawa Y and Sato K 2000 *Japan. J. Appl. Phys.* **39** L949
[5] Cho S, Choi S, Cha G B, Hong S C, Kim Y, Zhao Z Y, Freeman A J, Ketterson J B, Kim B J, Kim Y C and Cho B C 2002 *Phys. Rev. Lett.* **88** 257203
[6] Jaffe J E and Zunger A 1984 *Phys. Rev.* B **30** 741
[7] Zhao Y J and Zunger A 2004 *Phys. Rev.* B **69** 104422
Zhao Y J and Zunger A 2004 *Phys. Rev.* B **69** 075208
[8] Kamatani T and Akai H 2003 *Mater. Sci. Semicond. Process.* **6** 389
[9] Mahadevan P and Zunger A 2002 *Phys. Rev. Lett.* **88** 047205
[10] Picozzi S, Zhao Y J, Freeman A J and Delley B 2002 *Phys. Rev.* B **66** 205206
[11] Erwin S C and Zutic I 2004 *Nat. Mater.* **3** 410
[12] Zhao Y J, Picozzi S, Continenza A, Geng W T and Freeman A J 2002 *Phys. Rev.* B **65** 094415
[13] Picozzi S 2004 *Nat. Mater.* **3** 349
[14] Shay L J and Wernick J H 1975 *Ternary Chalcopyrite Semiconductors: Growth, Electronic Properties and Applications* (Oxford: Pergamon)
[15] Lind M D and Grant R W 1973 *J. Chem. Phys.* **58** 357
[16] Jaffe J E and Zunger A 1984 *Phys. Rev.* B **29** 1882 and references therein
[17] Van Leuken H and De Groot R 1995 *Phys. Rev. Lett.* **74** 1171
[18] Akai H and Ogura M 2006 *Phys. Rev. Lett.* **97** 026401
[19] Pickett W E 1998 *Phys. Rev.* B **57** 10613
[20] Wurmehl S, Fecher G H and Felser C 2006 *J. Phys.: Condens. Matter* **18** 6171
[21] Zunger A 1986 *Solid State Phys.* **39** 275
[22] Perdew J P, Burke K and Ernzerhof M 1996 *Phys. Rev. Lett.* **77** 3865
[23] Wimmer E, Krakauer H, Weinert M and Freeman A J 1981 *Phys. Rev.* B **24** 864
[24] http://www.flapw.de
[25] Monkhorst H J and Pack J D 1976 *Phys. Rev.* B **13** 5188
[26] Anisimov V I, Aryasetiawan F and Lichtenstein A I 1997 *J. Phys.: Condens. Matter* **9** 767
[27] Zhao Y J, Mahadevan P and Zunger A 2005 *J. Appl. Phys.* **98** 113901 and references therein
[28] Sato K, Dederichs P H, Katayama-Yoshida H and Kudrnovsky J 2004 *J. Phys.: Condens. Matter* **16** S5491